Vol. 87 No. 2 pp. 540–554 ACTA GEOLOGICA SINICA (English Edition) Apr. 2013

Jurassic Black Shales Facies from Qiangtang Basin (Northern Tibet): Rare Earth and Trace Elements for Paleoceanographic Implications

CHEN Lan[1, 2, 3, *], YI Haisheng[4, 5], TSAI Louis Loung-Yie[2], XU Guiwen[1], DA Xuejuan[1] and LIN Andrew Tien-Shun[3]

1 *College of Petroleum Engineering, Chongqing University of Science and Technology, Chongqing 401331, China*
2 *Institute of Applied Geology, National Central University, Jhongli 32001*
3 *Institute of Geophysics, National Central University, Jhongli 32001,*
4 *Institute of Sedimentary Geology, Chengdu University of Technology, Chengdu 610059, China*
5 *State Key Laboratory of Oil/Gas Reservoir Geology and Exploitation, Chengdu University of Technology, Chengdu 610059, China*

Abstract: The Biluo Co and Amdo 114 station, northern Tibet, cropping out the Early Toarcian and Middle-Late Tithonian (Jurassic) organic-rich black shales, have been a focus to petroleum geologists in discussing their oil-producing potential. This paper first reports the trace elements and rare earth elements to discuss the paleoenvironments, redox conditions and sedimentary mechanisms of those black shales. Both sections exhibit variation in trace element abundances with concentrations <0.1 ppm to 760 ppm, mostly enriched in V, Cr, Ni, Cu, Zn, Mo, Ba and U. Element ratios of Ni/Co, V/Cr, U/Th and V/(V+Ni) plus U were used to identify redox conditions. The shale-normalized rare earth element (REE) patterns are characterized by the flat-shale type with instable Ce anomalies and very weekly positive Eu anomalies. Positive Ce_{anom} values are significant with values varying between –0.064 and 0.029 in Biluo Co, which may be interpreted as release of REE and input of riverine terrestrial matter with rich Ce (resulting in pH change) during the anoxic conditions. In the middle parts of Amdo 114 station, distinct negative Ce_{anom} values are observed (−0.238 to −0.111) and associated surface water warming were interpreted as being related to a major sea level rise. In contrast, the formation of the black shales in the lower and upper part of the studied succession took place during a cooler (Ce_{anom} values >–0.10), lower surface water productivity, and lower sea-level stage. Thus, we emphasize the role of different factors that control the formation of local and regional black shales. The most important factors are sea-level fluctuations and increasing productivity.

Key words: Jurassic, black shale facies, rare earth and trace elements, paleoceanography, northern Tibet

1 Introduction

Black shales and/or black shales facies, visually identified by their color, were thinly carbonaceous shale, exceptionally rich in organic matter (5% or more carbon content) and sulfide (especially iron sulfide, usually pyrite), commonly contained unusual concentrations of certain trace elements (U, V, Cu, Ni) (Neuendorf et al., 2005), considered to record anoxic sedimentary environments (Vine and Tourtelot, 1970). Black sediments are deposited under a wide diversity of conditions: freshwater to estuarine to marine, incorporating varying organic productivity and sedimentary pH values. Because of the presence of common microcrystalline sulfide compounds (FeS (black) or FeS_2 (green)) and black minerals (Mn), the black color is not always an indicator of reduction conditions. Accordingly, the geochemical characteristics of black shales may record variations in environmental conditions of deposition. The bulk chemical composition of black shales reflects: (1) their initial (pre-erosional) source rocks; (2) the chemistry of the depositional environment; and (3) post-lithofaction processes (Quinby-Hunt and Wilde, 1994).

Jurassic or Cretaceous black shales in Europe, linked with the oceanic Anoxic Events (OAEs) (Jenkyns, 1988), were taken to reflect the effects of global, synchronous deposition without synchroneity being demonstrated. But

* Corresponding author. E-mail: cllc-10@163.com

the mechanisms to produce widespread anoxia are still under debate (Leckie et al. 2002; Meyers and Negri, 2003; Negri et al., 2006; Hofmann et al., 2008; Tiraboschi et al., 2009; Mazzini et a., 2010; Jenkyns, 2010). Thus, lithologically described black shales can be deposited under a variety of environmental conditions, which must be identified through means rather than simple color or paleontology or the preservation of organic matter or even isotopes ($\delta^{13}C$, $\delta^{18}O$, $\delta^{15}N$, $\delta^{98}Mo$). However, the rare earth, trace elements are also important to determine in differing environmental conditions such as functions of redox conditions, plate-tectonic depositional setting, organic productivity, which can be discerned in black shales from the concentration of major mobile elements (Brumsack, 2006; Piper and Calvert, 2009; Baioumy and Ismael, 2010; Zanin et al., 2010; Zhou et al., 2011).

The rare earth element (REE) characteristics including distribution, cerium and europium anomalies have been used to be potential indicators of depositional environments, for example, paleosalinity and water depth, pH and Eh of water mass, redox conditions, eustatic sea-level changes, and so on (Mazumdar et al., 1999; Guo et al., 2007; Zanin et al., 2010). Variations in the REE content in different lithologic types have been either attributed to varying depositional conditions, and the REE concentration patterns are primarily determined by the disintegration of the labile Fe-Mn-oxyhydroxide phase, originally precipitated from the water column (Wright et al., 1987). It is important to note that the presence in black shales of negative Ce anomalies typical of seawater may be a reliable redox indicator of the primary water body (Mazumdar et al., 1999).

To obtain insight into the formation of local and regional black shales and paleoenvironmental changes, we studied two black shale couplets the Biluo Co and Amdo 114 station of the Jurassic sections in Qiangtang Basin (northern Tibet, China). These black shales are both classic examples of oil-prone source rocks and have been a focus of scientific interest. Fu et al. (2008, 2010) discussed the REE characteristics, Re-Os dating, and sedimentary environments of marine oil shales in Shengli River-Changshe Mountain area, northern Tibet, but the above-mentioned black shales of Biluo Co and Amdo 114 station have been little mentioned in elemental geochemistry to understand the paleoceanographic implications. In recent years, some results have shown the Biluo Co shales deposited under reducing and anoxic conditions (Chen et al., 2005; Yin et al., 2006), but there has been continuing debate over whether anoxic conditions were persistent or seasonal, and whether the eustatic sea-level changes in shales of the anoxic facies can be supported by the trace elements, cerium anomaly, or the REE in marine black shales may reflect the redox conditions of ambient seawater.

In this paper, we attempted to explain the variable elemental anomalies, sea-level changes as well as the paleoceanographic implications in the black shales of Lower Toarcian and Middle-Upper Tithonian in Qiangtang Basin. The geochemical evolution in the organic-rich matter phases of two successions were also compared to discuss mechanisms responsible for the most organic carbon-rich black shales and caused oceanic anoxic events.

2 Geological Setting

2.1 Geological setting

Qiangtang Basin lies in between the Jinshajiang and Banggong-Nujiang suture zones (JSS and BNS) in the northern Qinghai-Tibet Plateau (Fig. 1a). Structurally, the basin is characterized by one uplift and two depressions from north to south: northern Qiangtang depression, central uplift, and southern Qiangtang depression, respectively (Fig. 1b). During the Late Triassic, the Indosinian orogeny caused the complex activities of the Xijinwulan-Jinshajiang fold and the opening of the Meso-Tethyan sea within the BNS (Li et al., 1996). After the opening of Meso-Tethys, the Qiangtang terrane moved and subducted northward. Two marine basins (the northern Qiangtang Basin and southern Qiangtang Basin, respectively) began to separate and developed. The southern Qiangtang Basin is characterized by a slope environment of a passive continental margin, while the northern Qiangtang Basin equates to a peripheral foreland basin environment. During the Jurassic, because of the new Tethyan sea opening in the Yarlung Zangbu zone, the Gondese-Tanggula terrane moved northward and the Banggong-Nujiang was gradually closed, which resulted in subcrustal lithosphere subduction toward the Qiangtang terrane as a result of island arc formation in the central uplift (Huang, 2000). Subsequently, the northern Qiangtang Basin gradually evolved into back-arc foreland land, while the southern Qiangtang area became a fore-arc basin.

Different subsidence rates originated in various sections of the Qiangtang Basin and, also due to variable sedimentation rate, marked paleoenvironmental differentiations occurred. The physiography of the sea bottom was developed into relative structural highs and troughs, connected by variously inclined slopes. Consequently, the Jurassic sedimentary sequences show a sharp variation in thickness and lithologies.

2.2 Litho- and biostratigraphy

The Bilong Co section crops out on the margin of the central uplift. The whole succession has been described in detail previously by Chen et al. (2005) with oil shales, shales, marls, and mudstones (Fig. 2a). Abundant ammonites at the top of the section include a specimen identified as an Early Toarcian *Harpoceras* sp., which was related to the global oceanic anoxic event during the peak of transgression in the Early Jurassic (Chen et al., 2005).

The Amdo 114 station section is located near the Qinghai-Tibet highway. The section provides good exposure with abundant ammonites and bivalves of Late Jurassic age (Chen et al., 2006). The lower part of this section is composed of sandstone, sandy gravel and siltstone, whereas the middle part is limestone, bioclastic and silty limestone. The upper part of the section is characterized by grey-green siltstone, calcareous fine-grained sandstone, dark grey, medium-thick bedded microcrystalline limestone, medium-thin bedded marl and bioclastic interbeds, partly as argillaceous and/or silty limestone (Fig. 2b). Fossils include bivalves *Buchia*, *Chlamys*, *Posidonia* plus some significant ammonites, which are typical of Middle-Late Tithonian (Late Jurassic).

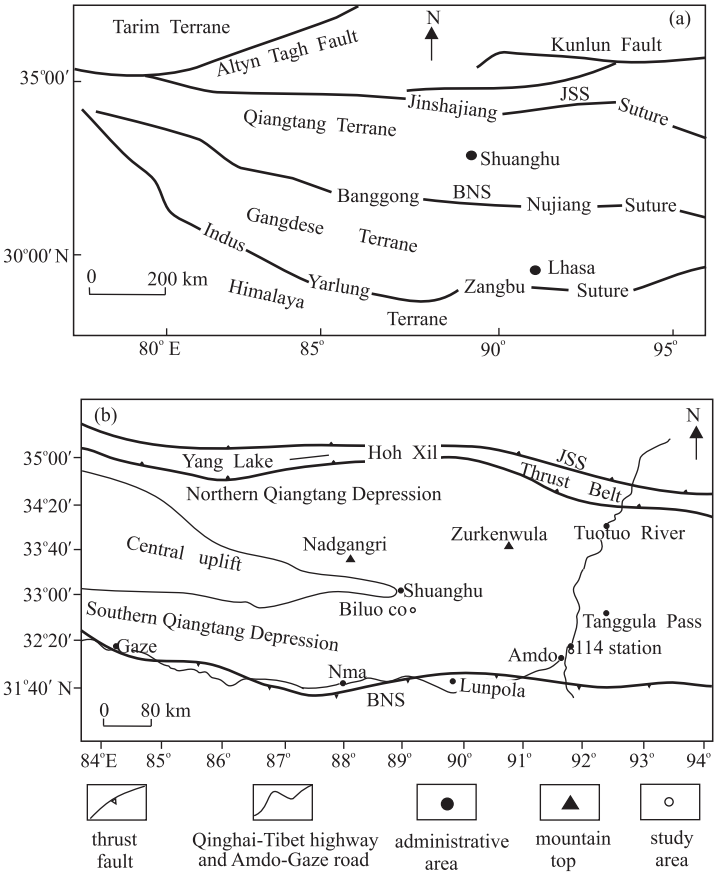

Fig. 1. Tectonic sketch map of the Qinghai-Tibet plateau (a) showing that the Qiangtang Basin is located between the Jingshajiang Suture and Bang-gong-Nujiang Suture. (b) Map showing the Qiangtang Basin tectonic units and the studied areas: Biluo Co and Amdo 114 station.

3 Sampling and Analytical Methods

Thirty-one organic-rich rock samples, 10 from the Biluo Co section and 21 from the Amdo 114 station section, were collected from outcrops in Qiangtang Basin, northern Tibet. These samples are mainly oil shales, shales, mudstones and marls with high organic carbon (Fig. 2). Whole-rock samples were trimmed to remove altered surfaces, and then cleaned with deionized water. All samples were crushed to 200 mesh for analysis of REE and trace element contents. Powdered samples were digested in a capped Teflon beaker with 1 mL ultrapure HF and 0.5 mL ultrapure HNO_3 at 200°C for 24 h until totally dissolved. After digestion of the powder, the vial was opened to air and heated to 130°C for 3 h until the sample was fully dried. The dried sample was finally diluted in 2 mL ultrapure HNO_3 and 5 mL ultrapure water. Dilute sample solutions were analyzed by a Perkin-Elmer Sciex ELAN 6000 inductively coupled plasma mass spectrometer (ICP-MS) at the State Key Laboratory of Ore Deposit Geochemistry, Institute of Geochemistry, Chinese Academy of Sciences (IGCAS), following procedures described by Qi et al. (2000). Analytical uncertainties are better than 5% for all elements based on the reproducibility of standards during the run analyses of international standards OU-6 and AHM-1 are in agreement with recommended values (Table 1 and Table 2).

Rare earth element data were normalized to the Post-Archean Australian Shale (PAAS) Standard (McLennan, 1989) to remove the odd-even effect of elemental abundances. Normalized REE abundances were then plotted on a logarithmic scale vs. atomic number on a linear scale.

4 Results

4.1 Trace elements

Trace elements distributions in representative samples from Biluo Co and Amdo 114 station black shales are shown in Table 1. Both sections exhibit variation in trace element abundances with concentrations <0.1 ppm to 760 ppm, except BP018b1 records 3004.579 ppm of Sr, however, the Ag, In, Hf, Ta, W, Ti and Bi are lower than <1 ppm. Their concentrations are lower than average

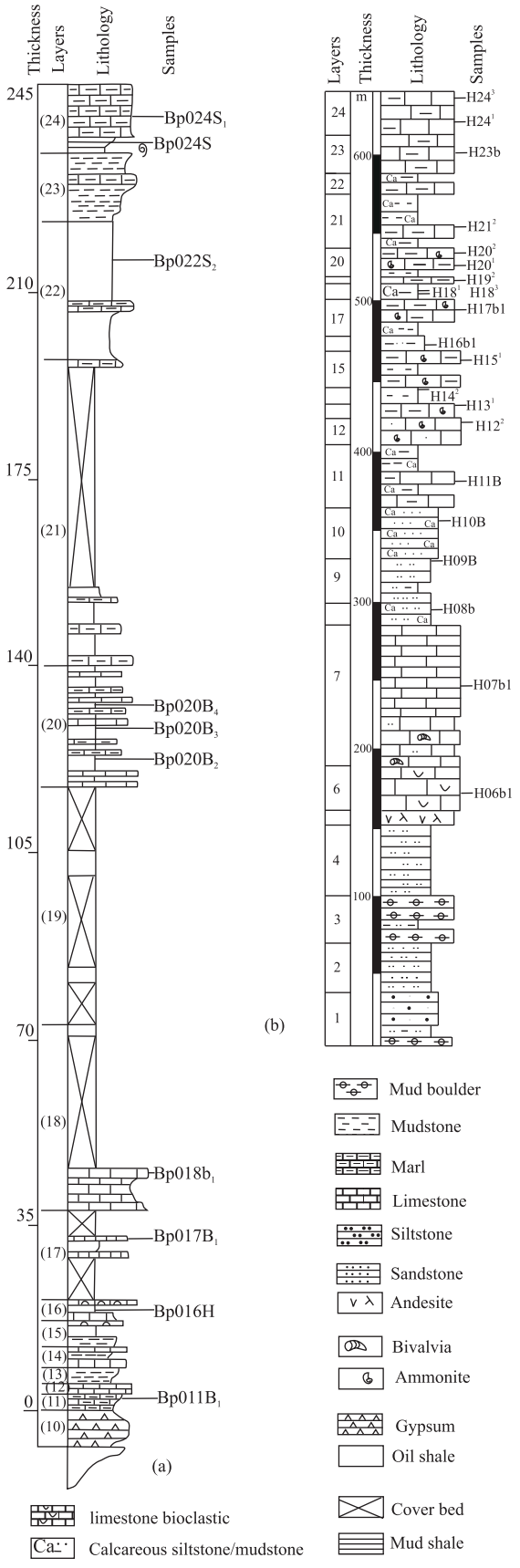

Fig. 2. The Lithostratigraphy of the Lower Toarcian in Biluo Co section (a) and the Middle-Upper Tithonian in Amdo 114 station section (b)

contents in black shales (Wedepohl, 1971, 1991). In the Biluo Co section, the concentrations of transition and chalcophile elements such as V, Cr, Ni, Cu, Zn, Mo, Ba and U in the lower part are extremely low compared with those of oil shales or marls. These elements are also strongly enriched in the oil shales of the middle part from BP020B2 to BP022B2, whereas the highest content occurred in the upper part. Similar enrichments of Sr and Ba are found in the carbonates of Biluo Co and Amdo 114 station. As shown in Table 1, the lower parts demonstrate the highest values of the V, Cr, Ni, Cu, Zn, Mo, Ba and U, with the lowest values of Sr in the whole profile. Furthermore, their concentrations exhibit obvious changes from lower to higher, and finally to lower.

4.2 Rare earth elements

The data on the REE contents in the black shales of the different locations and ages (Toarcian and Tithonian) are shown in the Table 2. The contents of REE in the black shales vary within close limits of 14.016–60.563 ppm, except H06b1 for 9.883 ppm and H07b1 for 3.741 ppm, and the average REE content in the main types of black shales is close to 30–50 ppm. The ΣREE values are lower than the average values reported from Jurassic black shales (Zanin et al., 2010; Baioumy and Ismael, 2010), also well below the world-average of black shales (131.45 ppm) (Yudovich and Ketris, 1994). The lithologic variation of the Biluo Co and Amdo 114 station displays not only in the total REE content, but also in ratios of LREE (La, Ce, Pr, Nd, Sm) to HREE (Eu, Gd, Tb, Dy, Ho, Er, Tm, Yb and Lu). In addition, the ΣLREE/ΣHREE rations vary from 6.6 to 9.6, which show the light REE (LREE) enrichments and heavy REE (HREE) depletion. The shale-normalized (McLennan, 1989) REE patterns are characterized by the flat-shale type with instable Ce anomalies and very weekly positive Eu anomalies (Fig. 3). Positive Ce_{anom} values are significant with values ranging between −0.064 and 0.029 in Biluo Co, whereas for the marls/limstones of Amdo 114 station the distinct negative Ce_{anom} values of −0.238 to −0.111 are observed. Eu anomalies fluctuate from 0.987 to 1.212 in Biluo Co and from 0.978 to 1.133 in Amdo 114 station with a mean value of 1.067, therefore, Eu/Eu^* exhibits no distinctive difference between two successions.

5 Discussion

5.1 Effect of depositional environment on trace elements

Organic-rich black shales have long been regarded as an indicator for anoxic depositional environment. Some major results have been precisely analyzed for those trace

Table 1 Trace elements concentration (in ppm) and some ratios values of the Jurassic black shales from Biluo Co and Amdo 114 station sections, northern Tibet

Location	Sample name	Lithology	Sc	V	Cr	Co	Ni	Cu	Zn	Ga	Ge	Rb	Sr	Zr	Nb	Mo	Ag	In	Sb
Biluo Co	BP024S1	Marl	4.243	41.344	37.090	4.799	26.255	7.010	41.676	7.279	0.532	68.184	588.612	48.912	5.388	1.151	0.238	0.026	1.297
	BP024S	Shale	4.559	42.505	42.943	5.652	30.826	7.240	41.121	7.451	0.507	68.323	588.334	49.175	5.338	1.069	0.219	0.024	1.348
	BP022B1	Oil shale	2.102	26.229	19.928	3.613	14.153	3.820	18.385	4.239	0.257	32.685	308.342	30.807	2.883	0.282	0.126	0.009	0.150
	BP020B4	Oil shale	1.532	40.898	20.175	3.019	13.867	2.382	17.681	2.820	0.202	23.672	421.509	34.685	2.450	0.444	0.134	0.005	1.418
	BP020B3	Oil shale	1.727	35.394	26.015	2.405	15.198	2.416	18.744	2.924	0.207	24.633	324.374	25.967	2.507	0.748	0.124	0.010	0.876
	BP020B2	Oil shale	2.424	49.419	27.587	4.068	15.935	3.324	21.775	4.225	0.313	35.832	307.501	32.268	3.182	1.390	0.127	0.013	N. d.
	BP018b1	Limestone	0.609	8.792	8.101	1.760	9.585	1.288	10.881	1.287	0.056	3.722	3004.579	10.906	1.084	0.575	0.018	N. d.	2.184
	BP017B1	Limestone	2.414	22.150	19.006	2.164	13.571	4.980	13.735	3.990	0.246	35.648	754.691	25.514	2.779	0.304	0.142	0.012	0.026
	BP016H	Oil shale	2.798	37.446	24.186	5.500	20.718	6.697	17.099	5.222	0.382	45.906	272.397	32.357	3.307	2.170	0.148	0.015	2.210
	BP011B1	Marl	1.570	17.475	11.380	2.201	11.632	1.951	9.740	2.470	0.191	19.690	411.711	15.918	1.557	0.188	0.023	0.016	0.866
Amdo 114 station	H24[3]	Argillaceous limestone	0.368	8.825	12.056	1.456	16.834	2.026	14.902	0.769	0.207	6.710	418.309	6.851	0.712	1.783	0.016	0.001	1.121
	H24[1]	Argillaceous limestone	1.927	17.751	18.213	3.310	17.380	3.353	12.688	3.345	0.271	30.069	389.541	19.900	2.211	0.734	0.148	0.010	0.888
	H23b	Argillaceous limestone	1.907	18.290	32.598	4.148	29.055	5.010	25.687	3.340	0.209	28.990	540.271	23.670	2.492	0.988	0.127	0.009	2.512
	H21[2]	Marl	1.612	14.642	20.655	2.372	17.603	2.647	18.953	2.834	0.201	23.921	586.532	23.013	2.133	0.957	0.103	0.004	1.467
	H20[2]	Marl	2.007	22.156	19.196	4.143	22.321	4.640	19.293	3.542	0.298	29.593	546.468	23.306	2.571	0.893	0.131	0.009	0.645
	H20[1]	Marl	2.122	21.036	18.961	4.368	21.439	4.948	17.573	3.582	0.249	31.530	585.411	23.441	2.392	0.795	0.142	0.010	1.186
	H19[2]	Marl	2.216	21.343	18.618	3.786	19.745	3.559	16.872	3.727	0.304	33.314	666.330	26.285	2.672	0.853	0.155	0.007	1.537
	H18[3]	Calcareous mudstone	2.514	22.654	21.610	4.344	23.106	4.730	16.267	4.225	0.334	35.612	553.762	38.055	3.491	1.820	0.141	0.009	0.090
	H18[1]	Calcareous mudstone	2.242	24.392	21.797	4.374	27.756	9.384	18.190	3.766	0.245	33.873	561.581	21.425	2.283	1.271	0.116	0.011	3.424
	H17b1	Marl	1.722	22.199	18.774	4.378	23.498	6.228	18.120	3.117	0.215	26.577	662.000	19.200	2.015	0.802	0.069	0.010	1.309
	H16b1	Silty mudstone	1.773	20.142	62.558	7.451	46.679	6.391	14.488	3.009	0.220	27.041	439.354	18.156	2.500	3.220	0.116	0.007	34.633
	H15[1]	Marl	2.846	30.464	25.999	5.743	29.391	8.167	20.197	4.812	0.333	41.747	418.736	29.504	3.093	1.540	0.157	0.015	4.587
	H14[2]	Mudstone	2.342	33.276	19.284	12.964	28.537	10.831	19.739	3.854	0.268	32.903	641.900	21.817	2.252	1.299	0.072	0.005	19.056
	H13[1]	Marl	1.683	18.564	18.233	10.584	25.364	5.542	21.984	2.830	0.169	26.417	536.362	16.588	1.756	1.097	0.025	0.008	1.028
	H12[2]	Limestone	1.283	14.146	15.554	3.254	20.034	2.557	15.923	2.167	0.143	18.815	497.797	17.230	1.586	0.887	0.059	0.007	3.160
	H11B	Marl	0.971	9.289	20.780	1.867	16.499	1.397	10.556	1.758	0.096	15.073	328.489	12.005	1.259	0.891	0.047	0.005	2.591
	H10B	Calcareous sandstone	1.104	10.291	11.788	1.579	10.206	1.609	12.591	1.741	0.119	16.165	414.176	11.889	1.292	0.730	0.053	0.003	1.546
	H09B	Siltstone	0.983	9.914	22.477	1.794	18.179	3.488	13.981	1.801	0.122	15.969	375.806	12.289	1.333	0.770	N. d.	0.006	1.732
	H08b	Calcareous siltstone	0.926	9.853	19.466	2.185	16.225	2.022	10.869	1.390	0.096	12.103	334.408	9.563	1.041	0.995	0.012	0.001	3.796
	H07b1	Micrite limestone	0.005	5.174	5.058	0.755	8.456	0.135	9.114	0.332	N. d.	2.838	251.574	3.405	0.252	0.257	N. d.	N. d.	0.222
	H06b1	Bioclastic limestone	0.362	6.703	8.902	1.573	12.677	1.237	9.570	0.939	0.043	7.957	263.002	5.294	0.578	0.491	0.213	0.003	2.173
Standard	OU-6	True	22.1	129.35	70.78	29.11	39.83	39.62	111.18	24.33	N. d.	120.2	130.89	174.15	14.79	N. d.	N. d.	N. d.	0.55
		Measured	22.820	132.648	65.055	30.096	43.046	38.620	108.314	23.337	2.079	111.682	122.290	162.085	13.695	0.455	0.780	0.082	3.194
	AHM-1	True	13.48	106.4	40.89	18.68	32.36	30.2	66.9	20.49	1.03	18.31	545.4	146	8.32	1.21	N. d.	N. d.	0.8
		Measured	13.250	111.897	44.146	19.535	34.564	29.799	68.018	19.322	1.109	16.947	507.944	133.362	7.514	0.850	0.701	0.036	0.043

Table 1 continued

Location	Sample name	Lithology	Cs	Ba	Hf	Ta	W	Tl	Pb	Bi	Th	U	U/Th	Sc/Th	V/(V+Ni)	Ni/Co	Sr/Ba	δU	V/Cr
Biluo Co	BP024S1	Marl	5.207	97.672	1.302	0.414	1.045	0.334	5.506	0.153	3.644	0.998	0.274	1.164	0.612	5.471	6.026	0.902	1.115
	BP024S	Shale	5.321	93.476	1.302	0.379	1.098	0.397	5.692	0.159	3.477	1.148	0.330	1.311	0.580	5.454	6.294	0.995	0.990
	BP022B1	Oil shale	2.634	79.709	0.761	0.207	0.665	0.147	2.972	0.082	2.137	0.798	0.374	0.984	0.650	3.918	3.868	1.057	1.316
	BP020B4	Oil shale	1.687	375.591	0.756	0.161	0.503	0.130	1.757	0.055	1.571	0.900	0.573	0.975	0.747	4.593	1.122	1.265	2.027
	BP020B3	Oil shale	1.690	68.078	0.652	0.180	0.566	0.146	1.871	0.053	1.606	1.853	1.154	1.076	0.700	6.318	4.765	1.552	1.361
	BP020B2	Oil shale	2.575	249.853	0.793	0.216	0.684	0.302	2.575	0.077	2.114	0.694	0.328	1.147	0.756	3.917	1.231	0.993	1.791
	BP018b1	Limestone	0.212	122.836	0.232	0.072	0.188	0.015	0.398	0.018	0.740	0.548	0.740	0.822	0.478	5.447	24.460	1.379	1.085
	BP017B1	Limestone	2.429	107.166	0.638	0.175	0.477	0.101	3.434	0.066	1.997	0.897	0.449	1.209	0.620	6.272	7.042	1.148	1.165
	BP016H	Oil shale	3.401	58.638	0.811	0.225	0.676	0.558	4.321	0.087	2.341	1.931	0.825	1.195	0.644	3.767	4.645	1.424	1.548
	BP011B1	Marl	1.290	116.286	0.350	0.113	0.269	0.085	1.334	0.032	1.187	0.796	0.671	1.323	0.600	5.284	3.541	1.336	1.536
Amdo 114	$H24^3$	Argillaceous limestone	0.967	17.032	0.176	0.048	0.233	0.170	1.146	0.023	0.585	2.718	4.648	0.628	0.344	11.562	24.560	1.866	0.732
	$H24^1$	Argillaceous limestone	6.253	42.991	0.541	0.173	0.555	0.173	3.084	0.058	2.025	1.473	0.727	0.952	0.505	5.251	9.061	1.372	0.975
	H23b	Argillaceous limestone	5.617	70.196	0.607	0.192	0.730	0.450	2.470	0.062	1.969	1.434	0.728	0.969	0.386	7.004	7.697	1.372	0.561
	$H21^2$	Marl	6.177	53.787	0.606	0.147	0.509	0.140	3.055	0.056	1.754	1.325	0.755	0.919	0.454	7.422	10.905	1.388	0.709
	$H20^2$	Marl	2.384	52.498	0.671	0.192	0.625	0.259	4.626	0.081	1.995	2.389	1.197	1.006	0.498	5.388	10.409	1.564	1.154
	$H20^1$	Marl	3.951	40.390	0.624	0.172	0.599	0.220	5.347	0.081	1.980	1.193	0.603	1.072	0.495	4.908	14.494	1.288	1.109
	$H19^2$	Marl	3.033	41.055	0.690	0.199	0.642	0.189	4.895	0.093	2.187	2.628	1.202	1.014	0.519	5.215	16.230	1.566	1.146
	$H18^3$	Calcareous mudstone	2.528	46.669	1.024	0.240	0.691	0.210	7.636	0.104	2.720	1.042	0.383	0.924	0.495	5.319	11.866	1.070	1.048
	$H18^1$	Calcareous mudstone	3.033	40.093	0.585	0.162	0.725	0.319	3.994	0.101	1.988	1.455	0.732	1.128	0.468	6.345	14.007	1.374	1.119
	H17b1	Marl	5.198	41.717	0.509	0.134	0.586	0.288	3.582	0.103	1.742	2.223	1.276	0.989	0.486	5.367	15.869	1.586	1.182
	H16b1	Silty mudstone	2.178	96.152	0.483	0.181	1.441	0.315	4.782	0.086	1.613	2.078	1.288	1.099	0.301	6.265	4.569	1.589	0.322
	$H15^1$	Marl	2.988	84.673	0.746	0.232	0.647	0.333	6.374	0.127	2.484	2.437	0.981	1.146	0.509	5.118	4.945	1.493	1.172
	$H14^2$	Mudstone	2.579	38.671	0.560	0.161	0.588	0.314	5.363	0.116	1.915	1.203	0.628	1.223	0.538	2.201	16.599	1.307	1.726
	$H13^1$	Marl	3.398	39.551	0.425	0.128	0.403	0.210	4.105	0.081	1.449	1.569	1.083	1.162	0.423	2.396	13.561	1.529	1.018
	$H12^2$	Limestone	1.499	72.919	0.444	0.120	0.478	0.137	2.823	0.056	1.303	1.537	1.179	0.985	0.414	6.157	6.827	1.559	0.909
	H11B	Marl	1.666	29.611	0.308	0.094	0.529	0.060	1.355	0.035	0.962	2.668	2.774	1.010	0.360	8.837	11.093	1.785	0.447
	H10B	Calcareous sandstone	1.221	154.239	0.335	0.091	0.361	0.055	1.530	0.021	0.891	1.493	1.676	1.240	0.502	6.462	2.685	1.668	0.873
	H09B	Siltstone	1.211	99.977	0.339	0.092	0.381	0.074	1.226	0.036	0.928	1.154	1.244	1.059	0.353	10.131	3.759	1.577	0.441
	H08b	Calcareous siltstone	0.922	116.731	0.230	0.073	0.427	0.039	1.971	0.042	1.016	1.403	1.381	0.912	0.378	7.424	2.865	1.611	0.506
	H07b1	Micrite limestone	0.419	4.538	0.083	0.019	0.127	0.014	0.215	0.010	0.206	2.384	11.594	0.026	0.380	11.207	55.433	1.944	1.023
	H06b1	Bioclastic limestone	1.299	61.746	0.141	0.045	0.303	0.045	1.273	0.017	0.514	1.078	2.099	0.704	0.346	8.059	4.259	1.726	0.753
standard	OU-6	True	8.02	477.24	4.7	1.06	N. d.	0.53	28.22	N. d.	11.51	1.96							
		Measured	7.601	495.404	5.065	1.050	2.512	0.621	28.718	0.389	11.641	2.032							
	AHM-1	True	0.24	322.3	3.7	0.64	N. d.	0.08	9.85	N. d.	2.64	0.89							
		Measured	0.199	327.732	3.715	0.546	0.506	0.078	9.667	0.038	2.477	0.797							

$$\delta U = \frac{U}{\frac{1}{2}(U + \frac{Th}{3})}$$

(Wignall, 1994). N.d., no data

Table 2 Rare earth element (REE) concentrations (in ppm) and some ratios values of the Jurassic black shales from Biluo Co and Amdo 114 station sections, northern Tibet

Location	Sample name	Lithology	La	Ce	Pr	Nd	Sm	Eu	Gd	Tb	Dy	Ho	Er	Tm	Yb	Lu	Y	ΣREE
Biluo Co	BP024S1	Marl	14.079	24.099	2.869	10.500	2.114	0.443	1.884	0.314	1.646	0.385	1.001	0.144	0.940	0.145	11.949	60.563
	BP024S	Shale	13.868	23.581	2.880	10.277	2.009	0.402	1.765	0.271	1.601	0.387	0.987	0.141	0.962	0.135	12.028	59.265
	BP022B1	Oil shale	7.462	14.740	1.690	5.958	1.164	0.225	0.936	0.153	0.815	0.181	0.509	0.069	0.524	0.070	5.166	34.496
	BP020B4	Oil shale	5.763	11.214	1.260	4.760	0.926	0.207	0.843	0.135	0.740	0.147	0.420	0.062	0.412	0.056	4.609	26.943
	BP020B3	Oil shale	7.015	13.594	1.574	6.174	1.345	0.297	1.261	0.189	1.058	0.219	0.610	0.083	0.490	0.070	7.165	33.979
	BP020B2	Oil shale	7.546	14.541	1.646	6.144	1.137	0.259	0.966	0.160	0.902	0.194	0.530	0.081	0.528	0.073	5.378	34.709
	BP018b1	Limestone	3.168	5.951	0.680	2.485	0.437	0.112	0.434	0.065	0.359	0.088	0.229	0.033	0.187	0.034	2.400	14.263
	BP017B1	Limestone	7.765	15.212	1.765	6.490	1.327	0.277	1.054	0.169	0.976	0.205	0.549	0.077	0.526	0.074	5.405	36.465
	BP016H	Oil shale	9.686	19.031	2.156	7.710	1.406	0.324	1.331	0.203	1.156	0.245	0.666	0.093	0.615	0.089	6.849	44.710
	BP011B1	Marl	9.629	21.366	2.254	8.462	1.781	0.405	1.719	0.267	1.482	0.325	0.787	0.108	0.633	0.090	8.676	49.312
Amdo 114 station	$H24^3$	Argillaceous limestone	3.586	4.717	0.663	2.608	0.508	0.114	0.542	0.080	0.473	0.114	0.289	0.041	0.243	0.039	4.462	14.016
	$H24^1$	Argillaceous limestone	7.056	11.977	1.418	5.363	1.066	0.235	1.049	0.155	0.870	0.200	0.520	0.074	0.488	0.075	6.418	30.544
	H23b	Argillaceous limestone	7.511	12.465	1.530	5.612	1.014	0.228	0.966	0.142	0.832	0.197	0.522	0.071	0.474	0.069	6.428	31.632
	$H21^2$	Marl	7.877	12.350	1.584	5.766	1.047	0.239	1.044	0.163	0.947	0.222	0.661	0.077	0.500	0.072	8.100	32.549
	$H20^2$	Marl	9.273	14.352	1.735	6.521	1.318	0.284	1.221	0.190	1.152	0.255	0.677	0.090	0.540	0.088	9.006	37.696
	$H20^1$	Marl	9.278	14.602	1.835	6.955	1.429	0.285	1.322	0.207	1.144	0.248	0.692	0.098	0.618	0.095	9.088	38.808
	$H19^2$	Marl	9.861	14.783	1.872	6.912	1.324	0.289	1.199	0.202	1.062	0.253	0.712	0.087	0.613	0.080	9.267	39.247
	$H18^3$	Calcareous mudstone	11.256	17.932	2.301	8.199	1.633	0.330	1.444	0.240	1.329	0.309	0.845	0.121	0.774	0.105	10.322	46.818
	$H18^1$	Calcareous mudstone	9.831	14.777	1.842	6.922	1.272	0.301	1.272	0.222	1.182	0.271	0.723	0.088	0.632	0.082	9.766	39.417
	H17b1	Marl	8.466	12.152	1.577	5.772	1.148	0.253	1.088	0.168	0.997	0.221	0.573	0.077	0.522	0.067	8.733	33.081
	H16b1	Silty mudstone	9.514	12.233	1.618	6.172	1.140	0.259	1.144	0.173	0.995	0.228	0.599	0.084	0.526	0.069	9.407	34.752
	$H15^1$	Marl	11.460	18.197	2.205	8.021	1.515	0.339	1.414	0.224	1.350	0.283	0.786	0.115	0.688	0.096	10.420	46.694
	$H14^2$	Mudstone	9.109	14.819	1.825	6.624	1.374	0.313	1.329	0.209	1.148	0.257	0.712	0.098	0.636	0.083	9.339	38.536
	$H13^1$	Marl	9.171	12.469	1.653	6.091	1.150	0.241	1.189	0.182	0.958	0.227	0.582	0.081	0.504	0.076	9.115	34.574
	$H12^2$	Limestone	9.883	11.183	1.617	6.212	1.106	0.235	1.135	0.189	1.032	0.226	0.593	0.085	0.495	0.063	9.581	34.055
	H11B	Marl	6.529	6.993	1.064	3.880	0.709	0.163	0.745	0.125	0.639	0.175	0.459	0.059	0.370	0.050	7.270	21.959
	H10B	Calcareous sandstone	6.275	7.314	1.046	3.941	0.730	0.167	0.823	0.125	0.646	0.164	0.436	0.055	0.363	0.050	7.305	22.134
	H09B	Siltstone	6.368	7.436	1.045	4.171	0.717	0.168	0.729	0.123	0.681	0.175	0.451	0.059	0.339	0.046	7.353	22.506
	H08b	Calcareous siltstone	4.533	7.056	0.865	3.337	0.708	0.159	0.677	0.101	0.530	0.138	0.331	0.043	0.294	0.042	4.823	18.814
	H07b1	Micrite limestone	0.800	1.471	0.171	0.672	0.135	0.030	0.131	0.020	0.126	0.025	0.080	0.007	0.063	0.009	0.837	3.741
	H06b1	Bioclastic limestone	2.214	4.150	0.458	1.716	0.318	0.076	0.316	0.049	0.225	0.047	0.134	0.023	0.140	0.018	1.714	9.883
Standards	OU-6	True	33	74.42	7.8	29.01	5.92	1.36	5.27	0.85	4.99	1.01	2.98	0.44	3	0.45	27.35	
		Measured	32.162	73.310	7.690	28.580	5.763	1.316	5.130	0.836	4.913	1.074	3.072	0.448	3.196	0.473	24.361	
	AHM-1	True	15.87	33.03	4.21	17.69	3.68	1.16	3.34	0.51	2.84	0.57	1.52	0.21	1.37	0.21	16.44	
		Measured	15.217	31.545	4.065	15.817	3.404	1.079	3.184	0.513	2.646	0.574	1.479	0.209	1.393	0.200	13.648	

Table 2 Continued

Location	Sample name	Lithology	ΣLREE	ΣHREE	ΣLREE/ΣHREE	La/Ce	La_n/Yb_n	Sm_n/Yb_n	La_n/Sm_n	Y/Y*	Pr/Pr*	La_n/Nd_n	Dy_n/Sm_n	Ce_{anom}	Eu/Eu^*
Biluo Co	BP024S1	Marl	54.105	6.459	8.377	0.584	1.105	1.143	0.967	1.196	1.061	1.190	0.923	-0.062	1.045
	BP024S	Shale	53.016	6.249	8.483	0.588	1.064	1.061	1.003	1.215	1.088	1.198	0.945	-0.064	1.005
	BP022B1	Oil shale	31.239	3.257	9.593	0.506	1.051	1.129	0.931	1.073	1.061	1.112	0.830	-0.008	1.014
	BP020B4	Oil shale	24.129	2.814	8.575	0.514	1.033	1.143	0.904	1.116	1.014	1.075	0.947	-0.020	1.103
	BP020B3	Oil shale	29.998	3.980	7.537	0.516	1.056	1.394	0.758	1.187	1.010	1.008	0.932	-0.030	1.072
	BP020B2	Oil shale	31.275	3.434	9.107	0.519	1.055	1.094	0.964	1.025	1.025	1.090	0.940	-0.022	1.163
	BP018b1	Limestone	12.834	1.429	8.979	0.532	1.248	1.186	1.052	1.074	1.040	1.131	0.974	-0.028	1.212
	BP017B1	Limestone	32.836	3.629	9.048	0.510	1.090	1.283	0.850	0.965	1.045	1.062	0.872	-0.018	1.101
	BP016H	Oil shale	40.313	4.397	9.169	0.509	1.163	1.162	1.001	1.026	1.047	1.115	0.975	-0.010	1.114
	BP011B1	Marl	43.899	5.413	8.110	0.451	1.122	1.429	0.785	0.997	0.985	1.010	0.987	0.029	1.091
Amdo 114 station	$H24^3$	Argillaceous limestone	12.196	1.820	6.699	0.760	1.090	1.063	1.026	1.532	1.103	1.220	1.105	-0.173	1.026
	$H24^1$	Argillaceous limestone	27.115	3.430	7.906	0.589	1.067	1.110	0.962	1.227	1.041	1.167	0.968	-0.068	1.047
	H23b	Argillaceous limestone	28.359	3.273	8.664	0.603	1.169	1.086	1.077	1.264	1.075	1.188	0.973	-0.075	1.084
	$H21^2$	Marl	28.863	3.686	7.831	0.638	1.162	1.063	1.093	1.408	1.103	1.212	1.073	-0.097	1.078
	$H20^2$	Marl	33.484	4.213	7.948	0.646	1.268	1.240	1.022	1.325	1.055	1.262	1.036	-0.098	1.055
	$H20^1$	Marl	34.384	4.424	7.773	0.635	1.109	1.175	0.943	1.361	1.069	1.184	0.949	-0.099	0.978
	$H19^2$	Marl	35.041	4.207	8.330	0.667	1.188	1.098	1.082	1.425	1.088	1.266	0.951	-0.111	1.079
	$H18^3$	Calcareous mudstone	41.651	5.167	8.061	0.628	1.073	1.072	1.001	1.283	1.116	1.218	0.965	-0.090	1.013
	$H18^1$	Calcareous mudstone	34.946	4.471	7.816	0.665	1.148	1.023	1.123	1.375	1.070	1.261	1.101	-0.111	1.113
	H17b1	Marl	29.368	3.712	7.911	0.697	1.198	1.118	1.071	1.485	1.106	1.302	1.029	-0.127	1.067
	H16b1	Silty mudstone	30.934	3.818	8.102	0.778	1.336	1.102	1.213	1.573	1.091	1.368	1.035	-0.169	1.066
	$H15^1$	Marl	41.738	4.957	8.421	0.630	1.230	1.119	1.099	1.345	1.074	1.268	1.057	-0.086	1.092
	$H14^2$	Mudstone	34.063	4.472	7.617	0.615	1.058	1.098	0.963	1.371	1.083	1.220	0.990	-0.081	1.090
	$H13^1$	Marl	30.776	3.799	8.101	0.736	1.343	1.158	1.159	1.557	1.113	1.336	0.988	-0.147	0.972
	$H12^2$	Limestone	30.237	3.818	7.919	0.884	1.473	1.135	1.298	1.581	1.131	1.412	1.106	-0.221	0.989
	H11B	Marl	19.337	2.622	7.374	0.934	1.302	0.973	1.339	1.719	1.191	1.493	1.069	-0.238	1.054
	H10B	Calcareous sandstone	19.472	2.662	7.315	0.858	1.274	1.020	1.250	1.781	1.138	1.413	1.050	-0.208	1.013
	H09B	Siltstone	19.904	2.602	7.648	0.856	1.388	1.075	1.291	1.693	1.093	1.355	1.127	-0.212	1.093
	H08b	Calcareous siltstone	16.658	2.156	7.727	0.643	1.138	1.223	0.931	1.413	1.047	1.206	0.889	-0.101	1.080
	H07b1	Micrite limestone	3.279	0.462	7.105	0.544	0.939	1.095	0.858	1.186	1.013	1.057	1.104	-0.047	1.063
	H06b1	Bioclastic limestone	8.932	0.951	9.393	0.534	1.166	1.153	1.011	1.330	1.010	1.145	0.838	-0.027	1.133

Notes: $Y/Y^*=2Y_n/(Dy_n+Ho_n)$(Bau and Dulski, 1996). $Pr/Pr^*=2Pr_n/(Ce_n+Nd_n)$(Bau and Dulski, 1996). Ce anomaly is calculated using the formula: $Ce_{anom}=\log[3Ce_n/(2La_n+Nd_n)]$ (Elderfield and Greaves, 1982), while the Eu anomaly is calculated: $Eu/Eu^*=Eu_n/(Sm_n\times Gd_n)^{0.5}$(Taylor and McLenan, 1985). The n stands for Post-Archean Australian Shale (PAAS) -normalized values.

elements accumulated in marine sediments (ancient or modern basins) or sedimentary rocks, with a diagnostic of deposition under oxic (Mn and Fe), suboxic (Cr, Re, U, and V), and fully anoxic bottom-water conditions (Mo, Cd, Cu, Zn) (Piper and Calvert, 2009). So, the concentrations and ratios of the redox-sensitive trace metals such as Mo, V, Ni, Cr, U, and Mn may yield powerful information linked to local or global variability of paleoredox environments (Brumsack, 2006; Guo e al., 2007; Piper and Calvert, 2009; Baioumy and Ismeal, 2010). Of course, the strong enrichments in Cd, Mo, V, Cu, Ni, (Bi), and Sb demonstrate that bio-accumulation and presence of H_2S in the water column and associated with sulfidation processes (Brumsack, 2006). Element ratios of Ni/Co, V/Cr, U/Th and V/(V+Ni) plus U have been used to identify anoxic water-column conditions during black shale depositions (Jones and Manning, 1994; Rimmer, 2004).

The bulk Ni:Co ratios change between 3.7 and 6.3 with average values of 5.1 in Biluo cuo, whereas between 2.2 and 11.56 with average values of 6.38 in Amdo 114 station (Table 1), which suggests the Ni/Co average rations are higher than 4.0. According to the V/Cr values, we can see the ratios are very low in both sections, varying from 1 to 2.0 in Biluo Co and from 0.3 to 1.7 in Amdo 114 station. The uptake of V by algae is discernible, albeit weakly, by its slight depletion in the photic zone. As for Cr, it precipitates as $Cr(OH)_3$, or is adsorbed onto settling particles, under mildly denitrifying to anoxic conditions, i.e., throughout the O_2 depleted region of the water column. Under oxic conditions, Cr is in the oxidized and more soluble CrO_4^{2-} valence state (Murray et al., 1983). Higher Ni/Co and V/Cr ratios relate to increasingly deficient oxygen levels during deposition (Jones and Manning, 1994), due to the relative easiness at which Ni and V is sequestered by organic matter in reducing sediments (Breit and Vanty, 1991). In addition, Cr and Co concentrations are thought to be a function of detrital content, and not influenced by redox conditions (Ross and Bustin, 2009).

The U and Th exhibit similar geochemical characteristics, except under oxidizing conditions (Rogers and Adams, 1976; Wedepohl et al., 1978; Wang et al., 2011). Arthur and Sageman (1994) suggested the U/Th ratio in marine black shales is sensitive to the relative inputs of Th-bearing clay minerals and U is fixed in sediments during early diagenesis in anoxic environments. The U/Th ratio can be used as a redox indicator with high values (>1.25) associated with anoxic environment and low values (<0.75) associated with oxic environment (Jones and Manning, 1994). As shown in Table 1, the black shales from the Amdo 114 station section display higher U/Th ratios (0.3–2.8) and δU values (1.00–1.94) than those from the Biluo Co section (0.30–0.83 and 0.90–1.55 for U/Th and δU, respectively), which may indicate a more anoxic environment in Amdo 114 station area than Biluo Co area.

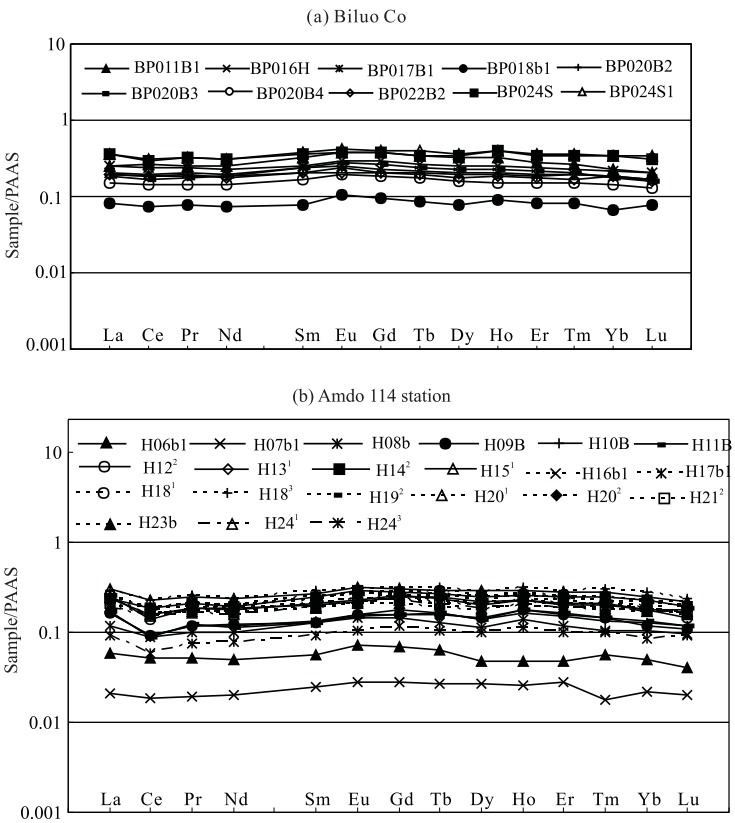

Fig. 3. Shale-normalized rare earth element (REE) distribution of black shales in Biluo Co (a) and Amdo 114 station (b).

The V/(V+Ni) ratio, or variation of the ratio, in bulk sediment has also been used to identify anoxic conditions in the geologic record. Enrichments of both metals were ascribed by Lewan and Maynard (1982) to the metallation of porphyrins, which are enriched in fine-grained shallow-water sediments with anoxic sediment in pore waters, but not necessarily deposited from anoxic bottom waters. Thus, variations in the V/(V+Ni) ratio could indicate relative changes in oxygenation with higher ratios signaling more strongly anoxic conditions of deposition. All black shales have similar values of V/(V+Ni) ratio from 0.3 to 0.8 in this study. As for a plot of U/Th vs V/(V+Ni) for these black shales (Fig. 4a), there is no distinct difference in two sections.

As mentioned previously, we can discuss the correlations among trace elements such as Mo, V, and U.

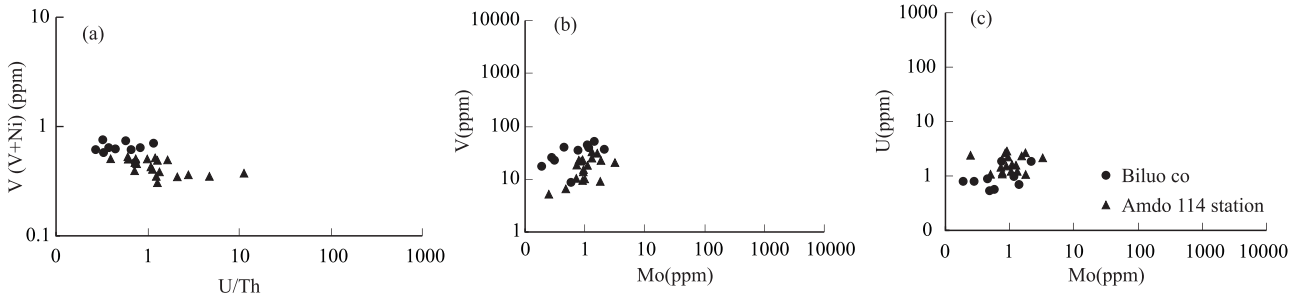

Fig. 4. The cross-correlation plots of selected trace elements for black shales in Biluo Co and Amdo 114 station.
(a) U/Th vs V/(V+Ni); (b) Mo vs V; (c) Mo vs U.

Fig. 4 shows the two profiles are similar with other anoxic basin (e.g., Saanich Inlet, Framvaren Fjord, the Cariaco Basin and the Black Sea), but absolute concentrations vary slightly. No correlations were observed between Mo vs V or U in the two sections (Fig.4 b,c). For example, Mo in the Black Sea possessed the highest concentration of ca. 75 nmol L^{-1} in the very surface water and decreased more or less uniformly to approximately 5 nmol L^{-1} at 300 m depth, below which it maintains a uniformly low concentration (Piper and Calveal, 2009). So, Tribovillart et al. (2008) have cautioned against the use of Mo enrichment as a proxy for bottom-water anoxia in ancient sediments in the absence of enrichments of other redox-sensitive trace elements such as Re, U, and V. Zheng et al. (2000) and McManus et al. (2006) further reported Mo accumulation under less anoxic conditions.

5.2 Rare earth element distributions

Shale-normalized REEs for black shales is shown in Fig. 3. The patterns exhibit LREE enrichment relative to HREE in all samples as shown by $(La/Yb)_N$ ratio of about 1.3. In Biluo Co, all samples have the similar REE distributions although the sample BP018b1 is slightly different. The two samples H06b1 and H07b1 of the Amdo 114 station show distinct difference from other samples. It is noted that not only Trace elements but REE are not in accordance with the general features in black shales (Zanin et al., 2010), which may indicate the different lithofacies and terrigenous source. According to Shengli River-Changshe Mountain oil shale zone, the ΣREE values range from 36.87 to 118.38 ppm, the LREE/HREE ratios between 6.79 and 10.74 (Fu et al., 2010). All results suggest a similar depositional environment and epigenetic evolution of shales, which deposited in the offshore to continental slope with slow sedimentary rate.

5.3 Cerium anomalies

Fractionation of cerium in seawater is apparently dependent upon redox potential. Changes in the value of the anomaly could be related to the redox conditions predicted by the ventilation model of Wilde (1987) with more negative values found during warmer climates and transgressive conditions and more positive values found during cooler to glacial climates and regressive conditions. According to Wright et al. (1987), the boundary between oxic and anoxic conditions is at Ce anomaly value of −0.10.

Ce anomalies with flat REE distribution and $(La/Sm)_N$ ratios >0.35 could be used as indicative of oceanic anoxia (Morad and Felitsyn, 2001). All samples with (La/Sm)n ratios >0.35–1.3 reveal no correlation with Ce anomaly, which indicates a true Ce anomaly with no infection on the diagenesis. Pr/Pr^* ratios average 1.035 and 1.084 in the Biluo Co and Amdo 114 station, respectively, which indicates that these Ce anomaly differences are subtle indeed and may have been artificially enhanced by variable La concentrations (Bau and Dulski, 1996).

Table 2 displays the Ce_{anom} values of the Jurassic black shales in the studied areas. Black shales in the Biluo Co are characterized by a positive Ce anomaly (having values from −0.064 to 0.029), which indicates the bottom water may be relatively oxic and is not accordant with the other results such as sedimentological, paleotological, tectonic and chemical information (Chen et al., 2005; Yin et al., 2006). This contradiction can be explained as follows: Under low oxygen conditions, the REE are released with the input of riverine terrestrial matter with rich cerium (resulting in pH change). Upon regeneration of this relatively Ce enriched authigenic phase, the released REE fraction would produce higher values of Ce_{anom}. This phenomenon is consistent with the positive Ce anomalies in the Atlantic ocean, anoxic Cariaco Trench (De Baar et al., 1985; 1988). The early Toarcian OAE is marked by a warming climate trend, which was probably related to increased CO_2 values (Hesselbo et al., 2000) and that was coupled to an enhanced hydrological cycle and riverine input, causing less saline surface waters, stratification and anoxic bottom water conditions in most NW European

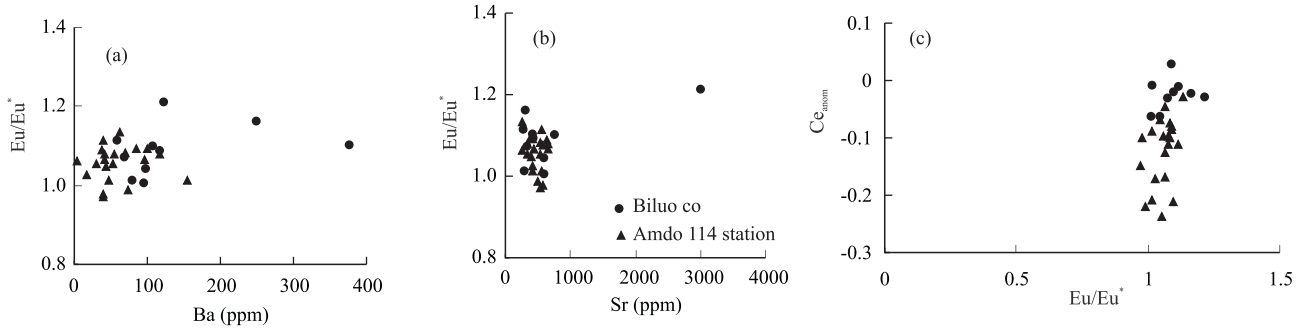

Fig. 5. Relationship between Eu anomalies and Ba, Sr and Ce anomalies in the Jurassic black shales. (a) Ba vs Eu/Eu*, (b) Sr vs Eu/Eu*, (c) Eu/Eu* vs Ce_{anom}.

epicontinental basins (Bonis et al., 2009; Mailliot et al., 2009). This may be occurring in the eastern Tethys, for example, Tibet. The organic carbon isotopes displayed a positive excursion of about 2.17‰ (PDB) in Biluo Co (Chen et al., 2005) and the abundant coccoliths occurred (Chen et al., 2006), which show the black shales of Early Toarcian are deposited in the transgressive conditions representing an anoxic environment.

In the Amdo 114 station, the Ce_{anom} values gradually decreased in the middle part. The Ce_{anom} values fell down to the lowest (−0.238 of H11B), then rose rapidly to about −0.1. The relatively stable values occurred in the upper part, but the values changed from −0.075 to −0.173 in the argillaceous limestones in the top part. As seen above, three sea-level falls and rises were identified on the base of the Ce anomalies in Amdo 114 station (Chen et al., 2012). From lower to upper, the relative eustatic sea-level changes are in regressive conditions indicating that the bottom water would become more oxic and the whole-rock Ce anomaly would be more positive, then in transgressive conditions indicating that the bottom water would become more anoxic and the whole-rock Ce anomaly would be more negative. Thus, we can conclude that the sea water is deepest in the middle part, which is in agreement with the appearance of abundant ammonites. Our results suggest that basinal sediments were not continuously anoxic and that a final model should accommodate to the chemical information.

5.3 Europium anomalies

Europium is believed to be the only REE, which may change its valency in a near surface environment (Brookins, 1989), whereby Eu^{3+} may be reduced to Eu^{2+} under extremely reducing conditions. The positive europium anomalies occur all black shales between 0.978 and 1.212 with a mean of 1.087. Previous analytical studies have shown that care must be taken into the interpretation of positive europisun anomalies measured by ICP-MS, due to various barium-compound interferences (Dulski, 1994). Unfortunately, some recent studies have drawn incorrect conclusions based on interference-related Eu anomalies, for example, Mazumdar et al. (1999), in which a rough Ba/(Eu/Eu*) correlation was interpreted to be of paleoenvironmental significance. Among the black shales studied, the weak correlation between Eu/Eu* and Ba confirms that no barium-compound interferences in this study (Fig. 5a). In addition, higher Ba concentrations varying from 17 ppm to 360 ppm indicate the higher productivity during the marine sedimentary processes. We also pay more attention to such correlations as Eu/Eu* and Sr or Ce_{anom} in all samples (Fig. 5b,c). There are no excellent linear correlations with the positive Eu anomalies, which further confirms that diagenetic processes or weathering have not altered the Eu anomalies of all samples in this study.

5.4 A proposed mechanism for Jurassic black shales

What could be the driving force for the local, regional or global occurrence of black shales during the Early Toarcian and Middle-Late Tithonian from geochemistry and calcareous nannofossils? Maybe this question is still open to debate. Currently available data suggest that the major forcing function behind OAEs was an abrupt rise in temperature, induced by rapid influx of CO_2 into the atmosphere from volcanogenic and/or methanogenic sources. Global warming was accompanied by an accelerated hydrological cycle, increased continental weathering, enhanced nutrient discharge to oceans and lakes, intensified upwelling, and an increase in organic productivity (Hermoso et al., 2009; Tiraboschi et al., 2009; Jenkyns, 2010; Herrle et al., 2010).

The two sets of Jurassic black shales in the Biluo Co and Amdo 114 station consist mostly of grey to dark-colores alternating oil shales, marls, mudstones, limestones and argillaceous limestones with lamination or horizontal bedding. Under the polarized light microscope

and scanning electron microscope (SEM), claystones are mostly of illite, chlorite, kaolinite and discrete pyrite. Long-term anoxic conditions are indicated by a general lack of benthic life but bloom of calcareous nannofossils (coccoliths), that is to say, the surface water had a condition featuring high productivity, while the anoxic bottom water had a condition unfavorable to benthic life. The Jurassic black shales in the studied areas have abundant calcareous nannofossils: *Watznaueria fossacincta* and *Watznaueria Britannica* (Chen et al., 2006), which have been linked to oxygen depletion, higher surface water productivity, and enhanced burial of organic matter. The importance of coccoliths in marine ecosystems and their widespread occurrence in the fossil record has led to the extensive use of nannofossil abundance and species diversity as proxies in paleo-temperature and nutrient availability in surface water (Herrle, 2003; Dunkley-Jones and Bown, 2007). In this study, the total nannofossil abundance and species diversity show lower values within the calcareous portion, compared to the argillaceous one and poor to moderate preservation (Chen et al., 2006). The oxygen isotope and Mg/Ca ratio recovered from belemnite guards indicate that the T-OAE is coeval with a 6–7°C warming of seawater (McArthur et al., 2000; Bailey et al., 2003; Gómez et al., 2008). A warmer climate caused higher wind speed, which increased surface water mixing and then increased surface water productivity. In contrast, a scenario of a cooler climate and higher surface water productivity is a more common element of icehouse conditions, where, for example, upwelling of cold and nutrient rich waters caused increasing surface water productivity (Herrle et al., 2010).

A number of redox-sentive trace metals are, with respect to average shales, concentrated in organic-rich sediments deposited during OAEs. The two sets of Jurassic black shales, northern Tibet, are characterized by higher enrichments in Ba and Mo, Ni, V, Cu, Cr, and U, reflecting the strong sulfidation in an anoxic water column. The stratigraphic distribution of some of these elements shows an initial peak, characteristic of the onset of the OAE, followed by a fall to very low values, indicating regional or possibly global drawdown of the geochemical species in question under anoxic to euxinic conditions and indicating the importance of the local environment (Hetzel et al., 2009).

As revealed in a past study of Biluo Co oil shales, the carbon isotope curve displays the $\delta^{13}C$ values of the kerogen fluctuating from −26.22‰ to −23.53‰ PDB with a positive excursion close to 2.17‰, which, albeit significantly smaller, may also have sea-level rise and has been associated with other Early Toarcian OAEs in Europe (Chen et al., 2005). Previous studies indicate that an inferred correlation of large positive $\delta^{13}C$ excursions and sea level rise may not be directly related and might be linked to other forcing factors that resulted in increased organic carbon burial (Bjerrum et al., 2006). Nevertheless, there is good evidence for a relationship between Ce with eustatic sea level changes (Wilde, 1987; Wilde et al., 1996; Yang et al., 1999). The ventilation model was predicted with more negative Ce anomaly values found during warmer climates and transgression conditions and more positive values found during cooler to glacial climates and regressive conditions. We interpret the long-term negative Ce_{anom} values(<-0.10) in the middle parts of Amdo 114 station section and associated surface water warming as being related to a major sea-level rise (Chen et al., 2012). In contrast, the formation of the black shales in the lower and upper part of the studied succession took place during a cooler (Ce_{anom} values >-0.10), lower surface water productivity, and lower sea-level. A sea-level change might have affected the water mass exchange and bottom ventilation (Herrle et al., 2010). Higher sea level probably enabled an enhanced exchange of water masses; therefore, the formation of the Biluo Co black shales was probably caused by increased productivity and organic matter flux, leading to enhanced preservation of organic material under surface waters. But the sedimentary mechanism of the gypsums in the lower part of the Biluo Co is still debatable and further studied. The lower and upper parts of the Amdo 114 station show a sea-level fall suggesting a restriction of water mass exchange. The reduced water mass exchange could have caused slightly reduced deep water formation and less mixing of surface water.

6 Conclusions

The Early Toarcian and Middle-Late Tithonian (Jurassic) black shales in Biluo Co and Amdo 114 station deposited under the oxygen-depleted conditions and lacked benthic life but had bloom of calcareous nannofossils. On the basis of trace elements and REE, these stratigraphic successions exhibit relative enrichments with Ba, Sr, Mo, V, Ni, Cr, Co, and U, while the REE is characterized by LREE enrichment, HREE depletion, and flat-shale type REE distribution of PAAS-normalized. The Ce anomalies indicate the sea level fluctuations in the studied successions. The formation of the Biluo Co and Amdo 114 station black shales couplets are caused by different mechanisms in accordance to the trace elements, rare earth elements and the calcareous nannofissils, including the sea level fluctuations and higher surface water productivity.

Acknowledgements

Thanks are extended to the Qinghai-Tibet research teams at Chengdu University of Technology for their kind help during our field investigation. In addition, we are grateful to Fu Shaohong, Institute of Geochemistry, Chinese Academy of Sciences, who carried out some laboratory works. Finally, this work was supported by Natural Science Foundation Project of CQ CSTC (Grant No. 2009BB7383), National Natural Science Foundation of China (Grant No. 41102066, 40972084) and Opening Foundation of the State Key Laboratory of Ore Deposit Geochemistry, Institute of Geochemistry, Chinese Academy of Sciences.

Manuscript received July 7, 2012
Accepted Dec. 2, 2012
edited by Fei Hongcai

References

Arthur, M.A., and Sageman, B.B., 1994. Marine black shales: depositional mechanisms and environments of ancient deposits. *Annual Review of Earth and Planetary Science*, 22: 499–551.

Bailey, L., Rosenthal, Y., McArthur, J.M., van de Schootbrugge, B., and Thirlwall, M.F., 2003. Paleoceanographic changes of the Late Pliensbachian-Early Toarcian interval: a possible link to the genesis of an oceanic Anoxic Event. *Earth and Planetary Science Letters*, 212: 307–320.

Baioumy, H.M., and Ismael, I.S., 2010. Factors controlling the compositional variations among the marine and non-marine black shales from Egypt. *International Journal of Coal Geology*, 83: 35–45.

Bau, M., and Dulski, P., 1996. Distribution of yttrium and rare-earth elements in the Penge and Kuruman iron-formations, Transvaal Suergroup, South Africa. *Precambrian Res.*, 79: 37–55.

Bjerrum, C.J., Bendtsen, J., and Legarth, J.J.F., 2006. Modeling organic carbon burial during sea-level rises with application to the Cretaceous. *Geochemistry, Geophysics, Geosystems*, 5, Q05008, 1–24.

Bonis, N.R., Ruhl, M., and Kürschner, W.M. 2009. Climate change driven black shales deposition during the end-Triassic in the western Tethys. *Palaeogeogr. Palaeoclimatol. Palaeoecol.*, doi:10.1016/j.palaeo.2009.06.016.

Breit, G.N., and Vanty, R.B., 1991. Vanadium accumulation in carbonaceous rocks: a review of geochemical controls during and deposition and diagenesis.*Chemical Geology*, 91: 83–97.

Brookins, D.G., 1989. Aquenous geochemistry of rare earth elements. In: Lipin, B.R., and McKay, G.A. (eds.), *Geochemistry and Mineralogy of Rare Earth Elements*. Min. Soc. Am., Rev. Mineral., 21, 221–225.

Brumsack, H.J., 2006. The trace metal content of recent organic carbon-rich sediments: Implications for Cretaceous black shale formation. *Palaeogeogr. Palaeoclimatol. Palaeoecol.*, 232: 344–361.

Chen Lan, Lin Andrew Tien-Shun, Da Xuejuan, Yi Haisheng, Tsai Louis Loung-Yie and Xu Guiwen, 2012. Sea-level change records by cerium anomalies of the Tithonian (Late Jurassic) black rock series in Qiangtang Basin, northern Tibet. *Oil shale*, 29(1): 18–35.

Chen Lan, Yi Haisheng, Hu Ruizhong, Zhong Hong and Zou Yanrong, 2005. Organic Geochemistry of the Early Jurassic Oil Shale from the Shuanghu Area in Northern Tibet and the Early Toarcian Oceanic Anoxic Event. *Acta Geologica Sinica* (English edition), 79(3): 392–397.

Chen Lan, Yi Haisheng, Zhong Hong, Hu Ruizhong, Yin Jiarun and Yang Jikai, 2006. A calcareous nannofossils record and its geological significance in the Jurassic black shales from the Qiangtang Basin, northern Tibetan Plateau. *Progress in Natural Science*, 16(special issue): 264–273.

De Baar, H.J.W., Bacon, M.P., Brewer, P.G., and Bruland, K.W., 1985. Rare earth elements in the Pacific and Atlantic Oceans. *Geochim. Cosmochim. Acta*, 49: 1943–1959.

De Baar, H.J.W., German, C.R., Elderfield, H., and Van Gaans, Pauline, 1988. Rare earth element distributions in anoxic waters of the Cariaco Trench. *Geochim. Cosmochim. Acta*, 52: 1203–1219.

Dulski, P., 1994. Interferences of oxide, hydroxide and chloride analyte species in the determination of rare earth elements in geological samples by inductively coupled plasma-mass spectrometry. *J. Anal. Chem.*, 350: 194–203.

Dunkley-Jones, T., and Bown, P.R., 2007. Post-sampling dissolution and the consistency of nannofossil diversity measures: a case study from freshly cored sediments of coastal Tanzania. *Marine Micropaleonotology*, 62: 254–268.

Elderfield, H., and Greaves, M.J., 1982. The rare earth elements distribution in seawater. *Nature*, 296: 214–219.

Fu Xiugen, Wang Jian, Qu Wenjun, Duan Taihong, Du Aandao, Wang Zhengjiang and Liu Hua, 2008. Re-Os (ICP-MS) dating of marine oil shale in the Qiangtang basin, northern Tibet, China. *Oil shale*, 25(1): 47–55.

Fu Xiugen, Wang Jian, Zeng Yuhong, Tan, Fuwen and Feng Xinglei, 2010. REE geochemistry of marine oil shale from the Changshe mountain area, northern Tibet, China. *International Journal of Coal Geology*, 81: 191–199.

Gómez, J.J., Goy, A., and Canales, M.L., 2008. Seawater temperature and carbon isotope variations in belemnites linked to mass extinction during the Toarcian (Early Jurassic) in Central and Northern Spain: Comparison with other European sections. *Palaeogeogr. Palaeoclimatol. Palaeoecol*., 258: 25–58.

Guo Qingjun, Shields, G.A., Liu Congqiang, Strauss, H., Zhu Maoyan, Pi Dahui, Goldberg, T., and Yang Xinlian, 2007. Trace element chemostratigraphy of two Ediacaran-Cambrian successions in South China: Implications for organosedimentary metal enrichment and silicification in the early Cambrian. *Palaeogeogr. Palaeoclimatol. Palaeoecol*., 254: 194–216.

Hermoso, M., Minoletti, F., Le Callonnec, L., Jenkyns, H.C., Hesselbo, S.P., Rickaby, R.E.M., Renard, M., de Rafélis, M., and Emmanuel, L., 2009. Global and local forcing of Early Toarcian seawater chemistry: A comparative study of different paleoceanographic settings (Paris and Lusitanian basins), *Paleoceanography*, 24, PA4208, doi:10.1029/2009PA001764.

Herrle, J.O., 2003. Reconstructing nutricline dynamics of mid-Cretaceous oceans: evidence from calcareous nannofossils

from the Niveau Paquier black shale (SE France). *Marine Micropaleontology*, 47: 307–321.

Herrle, J.O., Kössler, P., and Bollmann, J., 2010. Palaeoceanographic differences of early Late Aptian black shale events in the Vocontian Basin (SE France). *Palaeogeogr. Palaeoclimatol. Palaeoecol.*, doi: 10.1016/j.palaeo.2010.08.015.

Hesselbo, S.P., Gröcke, D.R., Jenkyns, H.C., Bjerrum, C.J., Farrimond, P., Morgans Bell, H.S., and Green, O.R., 2000. Massive dissociation of gas hydrate during a Jurassic oceanic anoxic event. *Nature*, 406: 392–395.

Hetzel, A., Böttcher, M.E., Wortmann, U.G., and Brumsack, H.J., 2009. Paleo-redox conditions during OAE 2 reflected in Demerara Rise sediment geochemistry (ODP Leg 207). *Palaeogeogr. Palaeoclimatol. Palaeoecol.*, 273: 302–328, doi: 10.1016/j.palaeo.2008.11.005.

Hofmann, P., Stüsser, I., Wagner, T., Schouten, S., and Sinninghe Damsté, J.S., 2008. Climateocean coupling off North-West Africa during the Lower Albian: The Oceanic Anoxic Event 1b. *Palaeogeogr. Palaeoclimatol. Palaeoecol.*, 262: 157–165.

Huang Jijun, 2000. Nature of the Qiangtang Basin and its tectonic evolution. *Journal of Geomechanics*, 6(4): 58–66 (in Chinese with English abstract).

Jenkyns, H.C., 1988. The Early Toarcian(Jurassic) anoxic event: Stratigraphic, sedimentary and geochemical evidence. *Am. J. Sci.*, 288: 101–151.

Jenkyns, H.C., 2010. Geochemistry of oceanic anoxic events. *Geochemistry, Geophysics, Geosystems*, 11, Q03004, doi:10.1029/2009GC002788.

Jones, B., and Manning, D.A.C., 1994. Comparison of geochemical indices used for the interpretation of paleoredox conditions in ancient mudstones. *Chemical Geology*, 111: 111–129.

Leckie, R.M., Bralower, T.J., and Cashman, R., 2002. Oceanic anoxicevents and plankton evolution: biotic response to tectonic forcing during the mid-Cretaceous. *Paleoceanography*, 17: 1–29.

Lewan, M.D., and Maynard, J.B., 1982. Factors controlling enrichment of vanadium and nickel in the bitumen of organic sedimentary rocks. *Geochimica et Cosmochimica Acta*, 46: 2547–2560.

Li Cai, He Zhonghua and Yang Deming, 1996. The Problems of Geological tectonics in the Qiangtang Area, Tibet. *Global Geology*, 15(3): 18–23 (in Chinese with English abstract).

Mailliot, S., Mattioli, E., Bartolini, A., Baudin, F., Pittet, B., and Guex, J., 2009. Late Pliensbachian–Early Toarcian (Early Jurassic) environmental changes in an epicontinental basin of NW Europe (Causses area, central France): a micropaleontological and geochemical approach. *Palaeogeography, Palaeoclimatology, Palaeoecology*, 273 (3–4): 346–364.

Mazumdar, A., Banerjee, D.M., Schidlowski, M., and Balaram, V., 1999. Rare-earth elements and stable isotope geochemistry of early Cambrian chert–phosphorite assemblages from the Lower Tal Formation of the Krol Belt (Lesser Himalaya, India). *Chem. Geol.*, 156: 275–297.

Mazzini, A., Svensen, H., Leanza, H.A., Corfu, F., and Planke, S., 2010. Early Jurassic shale chemostratigraphy and U-Pb ages from the Neuquén Basin(Argentina): Implications for the Toarcian Oceanic Anoxic Event. *Earth and Planetary Science Letters*, 297: 633–645.

McArthur, J.M., Donovan, D.T., Thirlwall, M.F., Fouke, B.W., and Mattey, D., 2000. Strontium isotope profile of the early Toarcian (Jurassic) oceanic anoxic event, the duration of ammonite biozones, and belemnite palaeotemperatures. *Earth and Planetary Science Letters*, 179: 269–285.

McLennan, S.M., 1989. Rare earth elements in sedimentary rocks: influence of provenance and sedimentary processes. In: Lipin B.R., and Mckay, G.A. (eds.), *Geochemistry and mineralogy of rare earth elements*. REV. Mineral., 21: 169–200.

McManus, J., Berelson, W.B., Severmann, S., Poulson, R.L., Hammond, D.E., Klikhammer, G.P., and Holm, C., 2006. Molybdenum and uranium geochemistry in continental margin sediments: paleoproxy potential. *Geochimica et Cosmochimica Acta*, 70: 4643–4662.

Meyers, P.A., and Negri, A., 2003. Paleoclimatic and paleoceanographic records in Mediterranean sapropels and Mesozoic black shales. *Palaeogeogr. Palaeoclimatol. Palaeoecol.*, 190: 5–6.

Morad, S., and Felitsyn, S., 2001. Identification of primary Ce-anomaly signatures in fossil biogenic apatite: implication for the Cambrian oceanic anoxia and phosphogenesis. *Sedimentary Geology*, 143: 259–264.

Murray, J.W., Spell, B., and Paul, B., 1983. The contrasting geochemistry of manganese and chromiumin the eastern tropical Pacific Ocean. In: Wong, C.S., Boyle, E., Bruland, K.W., and Goldberg, E.D. (eds.), *Trace Metals in Seawater, NATO Conference Series IV*. Plenum Press, New York, 643–669.

Negri, A, Wagner, T., and Meyers, P.A., 2006. Causes and consequences of marine organic carbon burial trough time. *Palaeogeogr. Palaeoclimatol. Palaeoecol.*, 235: 5–6.

Neuendorf, K.K.E., Mehl Jr., J.P., and Jackson, J.A. (eds.), 2005. Glossary of Geology, 5th ed.. *Am. Geol. Inst., Alexandria, Va.*, 72.

Piper, D.Z., and Calvert, S.E., 2009. A marine biogeochemical perspective on black shale deposition. *Earth-Science Reviews*, 95: 63–96.

Qi Liang, Hu Jing and Grégoire, D.C., 2000. Determination of trace elements in granites by inductively coupled plasma mass spectrometry. *Talanta*, 51: 507–513.

Quinby-Hunt, M.S., and Wilde, P., 1994. Thermodynamic zonation in the black shale facies based on iron-manganese-vanadium content. *Chemical Geology*, 113: 297–317.

Rimmer, S.M., 2004. Geochemical paleoredox indicators in the Devonian–Mississippian black shales, Central Appalachian Basin (USA). *Chemical Geology*, 206: 373–391.

Rogers, J.J.W., and Adams, J.A.S., 1976. *Handbook of Thorium and Uranium Geochemistry*. Beijing: Atomic Press (in Chinese).

Ross, D.J.K., and Bustin, R.M., 2009. Sediment geochemistry of the Lower Jurassic Gordondale Member, northeastern British Columbia. *Bulletin of Canadian Petroleum Geology*, 54: 337–365.

Taylor, S.R., and McLennan, S.M., 1985. The continental crust: its composition and evolution. *Blachwell, Oxford*, pp. 312.

Tiraboschi, D., Erba, E., and Jenkyns, H.C., 2009. Origin of rhythmic Albian black shales (Piobbico core, central Italy): Calcareous nannofossil quantitative and statistical analyses and paleoceanographic reconstructions. *Paleoceanography*, 24, PA2222,doi:10.1029/2008PA001670.

Vine, J.D., and Tourtelot, E.B., 1970. Geochemistry of black shale deposits-a summary report. *Econ. Geol.*, 65: 253–272.

Wang Xiang, Williams, L.G., Chen Jie, Huang Pinyun and Li Xiang, 2011. U and Th contents and Th/U ratios of zircon in felsic and mafic magmatic rocks: improved zircon-melt distribution coefficients. *Acta Geologica Sinica* (English edition), 85(1): 164–174.

Wedepohl, K.H., 1971. Environmental influences on the chemical composition of shales and clays. In: Ahrens, L.H., Press, F., Runcorn, S.K., and Urey, H.C. (eds.), *Physics and Chemistry of the Earth*, vol. 8. Pergamon, Oxford, 305–333.

Wedepohl, K.H., 1991. The composition of the upper earth's crust and the natural cycles of selected metals. Metals in natural raw materials. Natural Resources. In: Merian, E. (ed.), *Metals and Their Compounds in the Environment*. VCH, Weinheim, 3–17.

Wedepohl, K.H., Correns, C.W., Shaw, D.W., Turekian, K.K., and Zemann, J., 1978. *Handbook of Geochemistry*, vol.1–11 (1–5). Springer-Verlag, New York.

Wignall, P.B., 1994. Black shales. *Clarendon Press, Oxford*, 127.

Wilde, P., 1987. Model of progressive ventilation of the Late Precambrian-Early Paleozoic Ocean. *Am. J. Sci.*, 287: 442–459.

Wilde, P., Quinby-Hunt, M.S., and Erdtmann, B.D., 1996. The whole-rock cerium anomaly: a potential indicator of eustatic sea-level changes in shales of the anoxic facies. *Sedimentary Geology*, 101: 43–53.

Wright, J., Schrader, H., and Holser, W.T., 1987. Paleoredox variations in ancient oceans recorded by rare earth elements in fossil apatite. *Geochim. Cosmochim. Acta*, 51: 637–644.

Yang Jiedong, SunWeiguo, Wang Zongzhe, Xue Yaosong and Tao Xiaocong, 1999. Variations in Sr and C isotopes and Ce anomalies in successions from China: evidence for the oxygenation of Neoproterozoic seawater? *Precambiran Research*, 93: 215–233.

Yin Jiarun, Gao Jinhan, Wang Yongsheng, Zhang Shuqi, Zheng Chunzi, Xu Debiao, Bai Zhida, Sun Lixin and Su Xin, 2006. Jurassic ammonites in anoxic black shales from Sewa and Amdo, northern Tibet. *Acta Palaeontologica Sinica*, 45(3): 311–33 (in Chinese with English abstract).

Yudovich, Ya.E., and Ketris, M.P., 1994. Trace elements in black shales. *Nauka Publ., Ekaterinburg* (in Russian).

Zanin, Y.N., Eder, V.G., Zamirailova, Al.G., Krasavchikov, V.O., 2010. Models of the REE distribution in the black shale Bazhenov Formation of the West Siberian marine basin, Russia. *Chemie Erde-Geochemistry*, doi:10.1016/j.chemer.2010.04.001.

Zheng, Y., Anderson, R.F., Van Geen, A., and Kuwabara, J., 2000. Authigenic molybdenum formation in marine sediments: a link to pore water sulfide in the Santa Barbara Basin. *Geochimica et Cosmochimica Acta*, 64: 4165–4178.

Zhou Jiaxi, Huang Zhilong, Zhou Guofu, Li Xiaobiao, Ding Wei and Bao Guangping, 2011. Trace elements and rare earth elements of sulfide minerals in the Tianqiao Pb-Zn ore deposit, Guizhou Province, China. *Acta Geologica Sinica* (English edition), 85(1): 189–199.